Electronic Supplementary Material (ESI) for Materials Chemistry Frontiers.

Electronic Supporting Information

Surface defect-regulated PdCu/TiO_{2-x} promoting efficient electrocatalytic nitrogen reduction

Chengguang Liu, [a] Xiaolei Guo, [a] Zhen-Feng Huang,*[a] Jinheng Li, [a] Li Gan, [a] Lun Pan, [a] Chengxiang Shi, [a] Xiangwen Zhang, [a] Guidong Yang [b] and Ji-Jun Zou*[a]

[a] Key Laboratory for Green Chemical Technology of the Ministry of Education, School of Chemical Engineering and Technology, Tianjin University, Tianjin 300072, P. R. China; Collaborative Innovative Center of Chemical Science and Engineering (Tianjin), Tianjin 300072, P. R. China; Zhejiang Institute of Tianjin University, Ningbo, Zhejiang, 315201, P. R. China.

[b] XJTU-Oxford Joint International Research Laboratory of Catalysis, School of Chemical Engineering and Technology, Xi'an Jiaotong University, Xi'an 7010049, China.

* Corresponding author. E–mail: jj_zou@tju.edu.cn and zfhuang@tju.edu.cn

Experimental Section

NH_3 quantification

The quantitative detection of NH_3 concentration in solution was based on indiophenol blue coloration method.[1,2]. Specifically, 2 mL cathode electrolyte and 2 mL absorption solution were collected, then 2mL chromogenic reagent containing salicylic acid (5 wt%), sodium citrate (5 wt%) and 1 mol/L NaOH solution was added, followed by adding 1mL NaClO solution (0.05 mol/L). and finally, 200 μL sodium nitroferricyanide solution (1 wt%) was added and then shaken slightly. The absorbance data of the UV-vis absorption spectra were measured on the UV-1800 spectrophotometer after standing the mixed solution in the dark and reacting for 2 h at room temperature. To further quantitative calculation, the absorbance (Abs, a.u.) of a series of standard NH_4Cl solutions (c, μg mL^{-1}) with specified concentrations at λ = 655 nm were recorded in advance. The NH_4^+ standard curve in 0.1 mol/L HCl is y = 0.361x + 0.036 (R^2 = 0.999).

N_2H_4 quantification

The quantitative detection of N_2H_4 concentration in solution was based on the method of Watt and Chrisp.[3,4] A mixture of 5.99 g $C_9H_{11}NO$, 30 mL hydrochloric acid and 300 mL ethanol was used as an indicator. Afterward, 2 mL cathode electrolyte and 2 mL absorption solution were collected, followed by adding 2 mL of indicator into above solutions, respectively. The corresponding absorbance at λ = 455 nm were measured after at 10 min at room temperature Similarly, The N_2H_4 standard curve in 0.1 mol/L HCl was measured in advance, and the curve is y = 0.730x + 0.022 (R^2 = 0.999).

^{15}N isotope labeling experiment

When $^{15}N_2$ (99%, Shanghai Aladdin Biochemical Technology Co., LTD.) was used as the only feed gas, the produced NH_3 was determined by ^1H NMR spectra, using to further verify the N source of the produced NH_3. Before the electrochemical measurement, $^{15}N_2$ was immersed in the electrolyte for 1h until saturation. 500 μL of the electrolyte after electrolysis at –0.1 V *vs.* RHE was collected and 50 μL of DMSO-D6 was added, and then determined by a ^1H NMR spectrometer. Furthermore, the same procedure was used to detect $^{14}NH_3$ produced, apart from $^{14}N_2$ (99.999 %) as the feed gas.

Computational criterion

The NH_3 yield rate was calculated as follows equation:

NH_3 yield rate = $(c(NH_4^+) \times V) / (m_{cat} \times t)$

where $(c(NH_4^+)$ is the concentration of NH_4^+ determinedby indophenol blue method, quantitatively. V is the volume of the electrolyte, m_{cat} is the mass of the catalyst and t is the reduction time.

The Faradaic efficiency was estimated by the ratio of the charge consumed for NH_3 production to the total charge passing through the circuit. It was calculated according to following equation:

$FE = 3 \times F \times c(NH_4^+) \times V / (17 \times Q)$

where F is the Faraday constant (96485 C mol^{-1}), $c(NH_4^+)$ is the concentration of NH_4^+ determinedby indophenol blue method, quantitatively. V is the volume of the electrolyte and Q is the quantity of applied electricity.

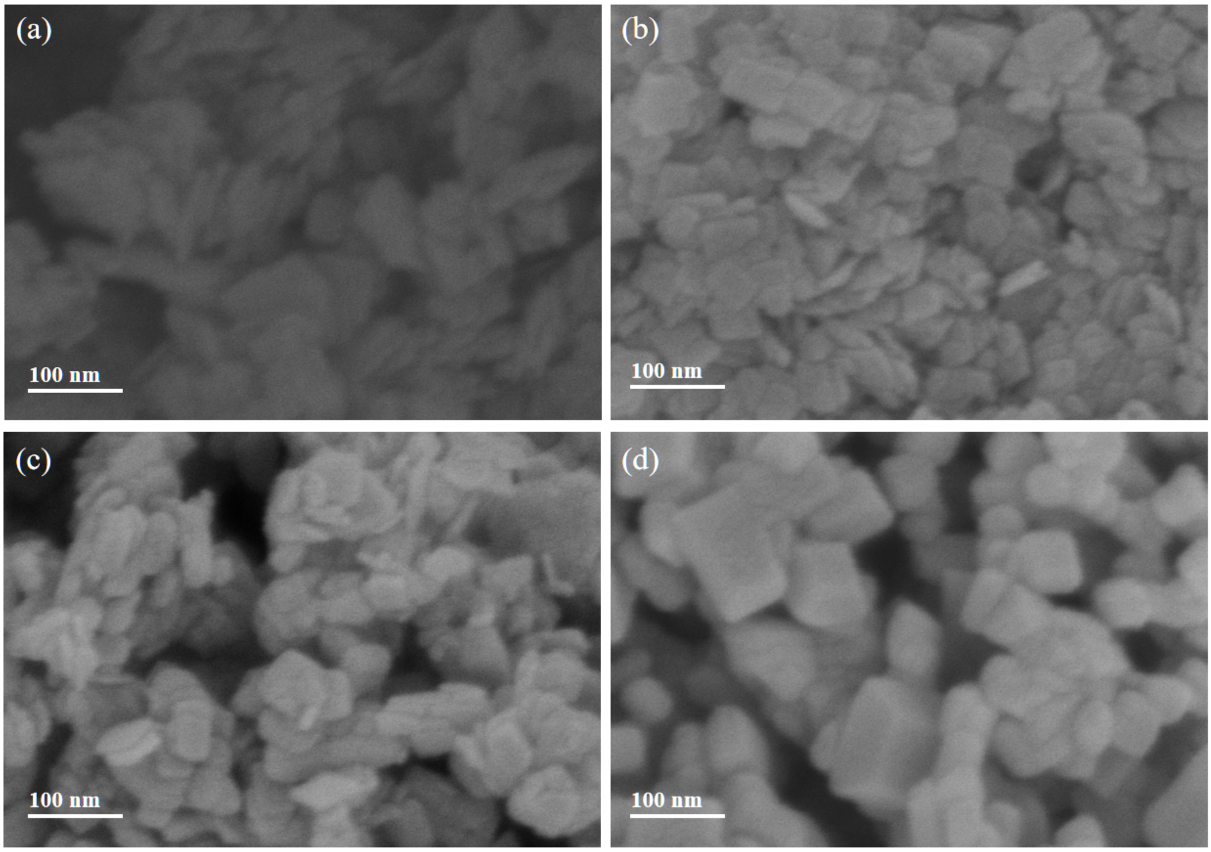

Fig. S1. SEM images of pristine TiO_2 and TiO_{2-x}-T (T = 200, 400, 600). (a) SEM image of TiO_2; (b) SEM image of TiO_{2-x}-200; (c) SEM image of TiO_{2-x}-400; (d) SEM image of TiO_{2-x}-600.

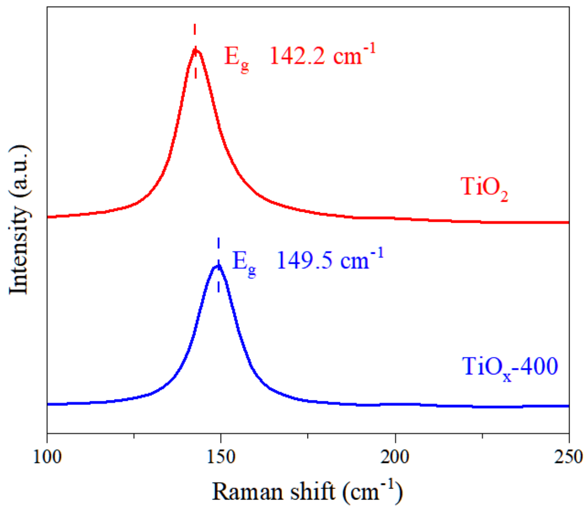

Fig. S2. Raman spectra of pristine TiO_2 and TiO_{2-x}-400.

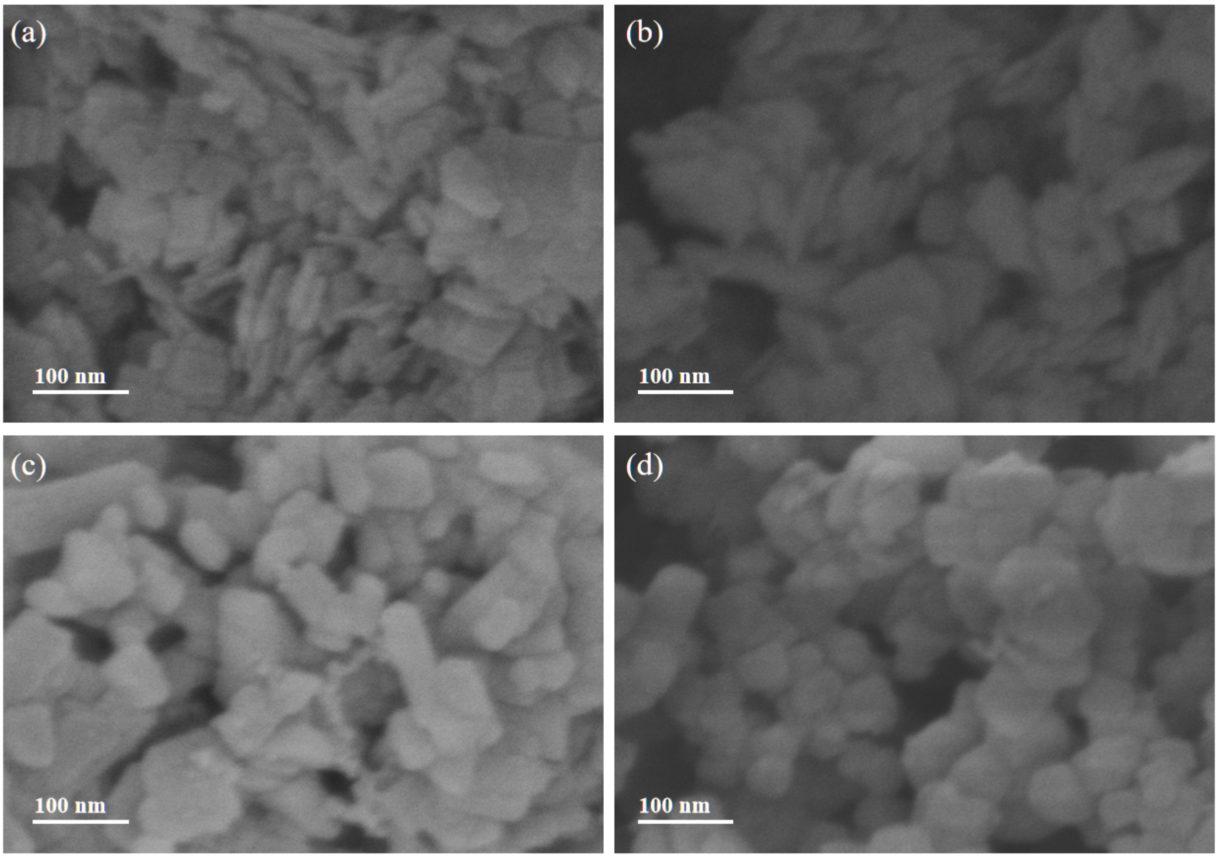

Fig. S3. SEM images of Pd_1Cu_1/TiO_2 and $Pd_1Cu_1/\ TiO_{2\text{-}x}$-$T$ (T = 200, 400, 600). (a) SEM image of Pd_1Cu_1/TiO_2; (b) SEM image of $Pd_1Cu_1/TiO_{2\text{-}x}$-200; (c) SEM image of $Pd_1Cu_1/TiO_{2\text{-}x}$-400; (d) SEM image of $Pd_1Cu_1/TiO_{2\text{-}x}$-600.

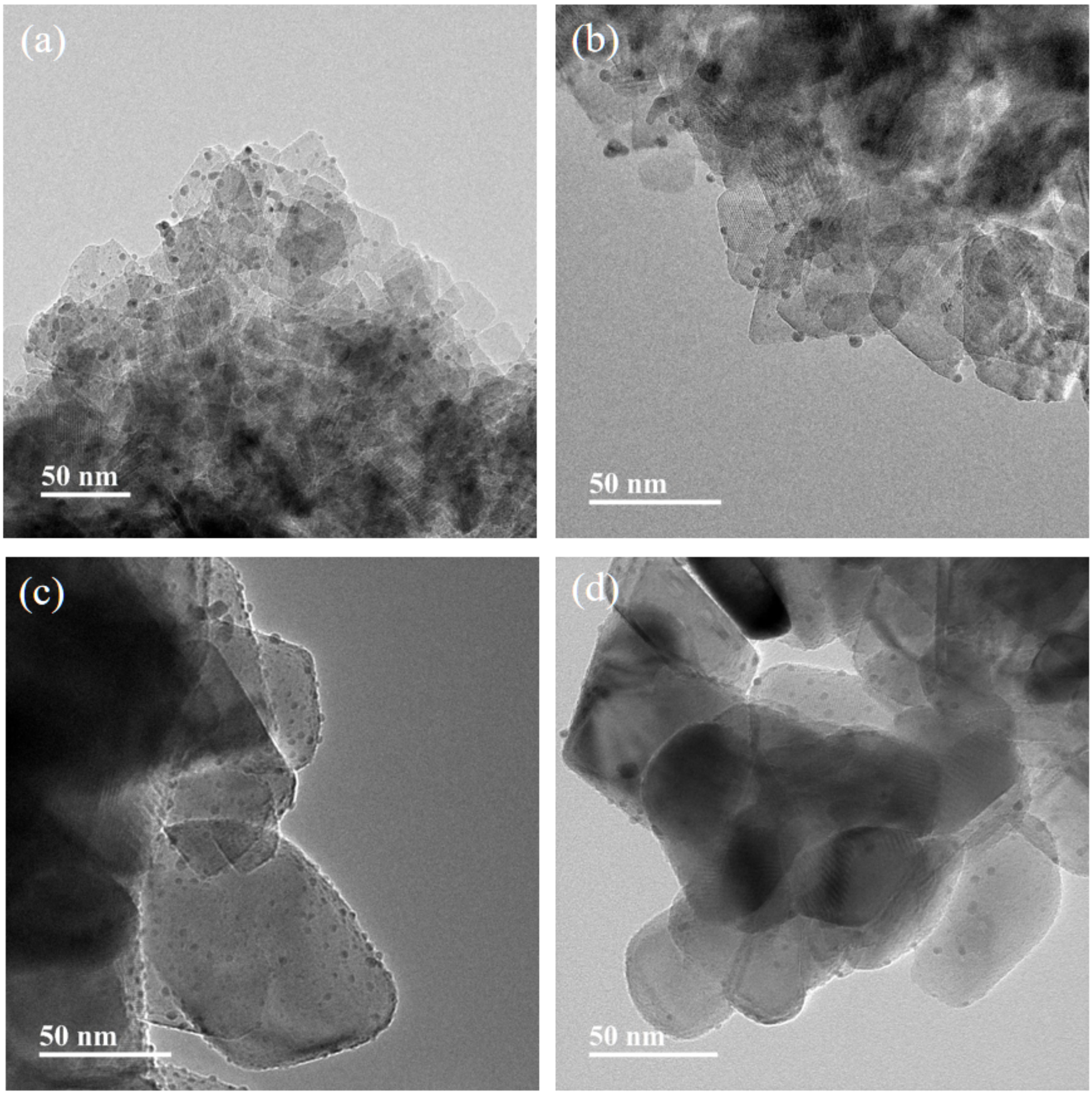

Fig. S4. (a) TEM image of Pd_1Cu_1/TiO_2; (b) TEM image of Pd_1Cu_1/TiO_{2-x}-200. (c) TEM image of Pd_1Cu_1/TiO_{2-x}-400; (d) TEM image of Pd_1Cu_1/TiO_{2-x}-600.

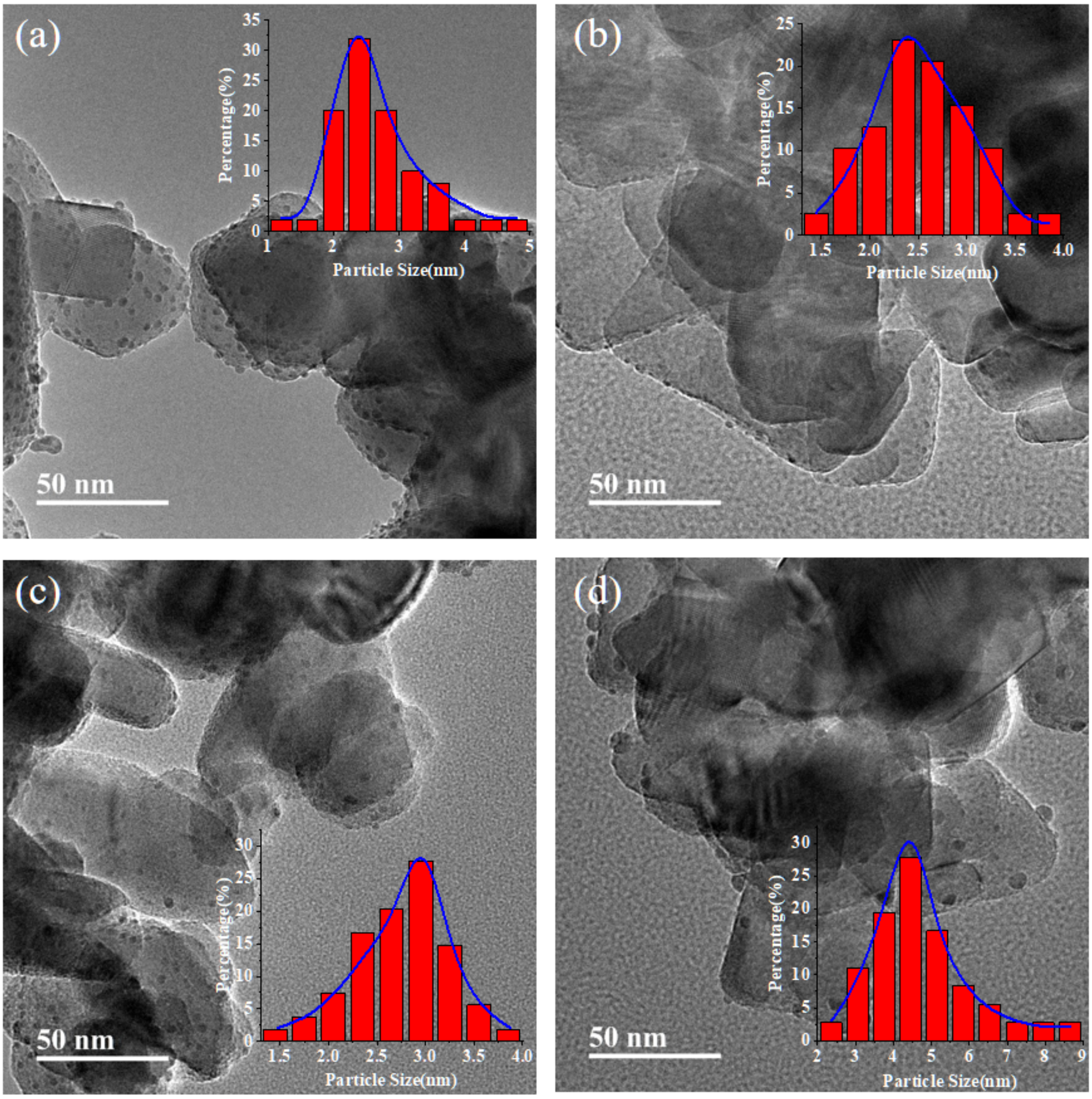

Fig. S5. TEM images of Pd_xCu_y/TiO_{2-x}-400. (a) TEM image of Pd/TiO_{2-x}-400; (b) TEM image of Pd_2Cu_1/TiO_{2-x}-400; (c) TEM image of Pd_1Cu_2/TiO_{2-x}-400; (d) TEM image of Cu/TiO_{2-x}-400.

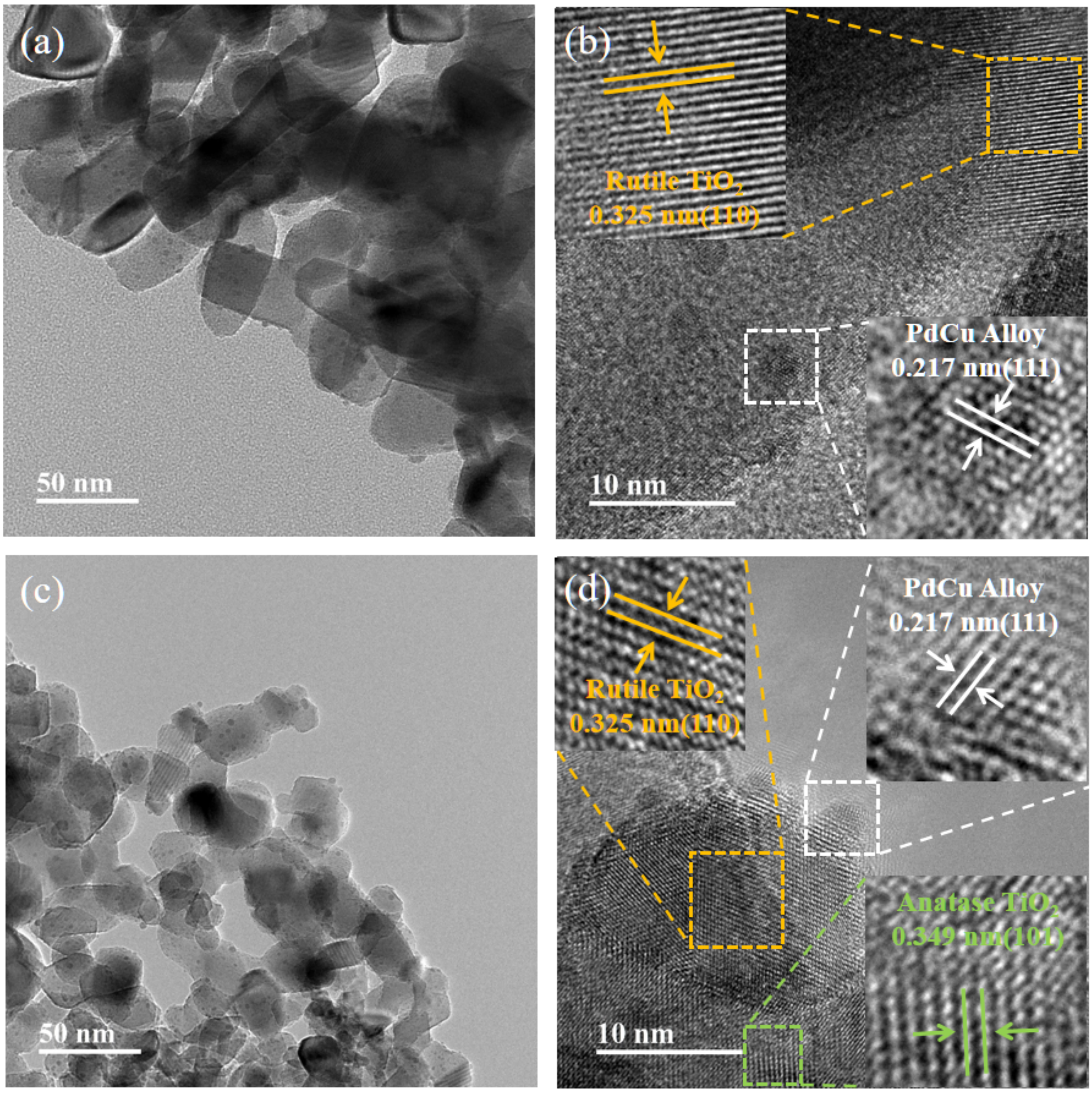

Fig. S6. (a, b) TEM and HRTEM images of Rutile Pd_1Cu_1/TiO_{2-x}-400; (c, d) TEM and HRTEM images of P25 Pd_1Cu_1/TiO_{2-x}-400.

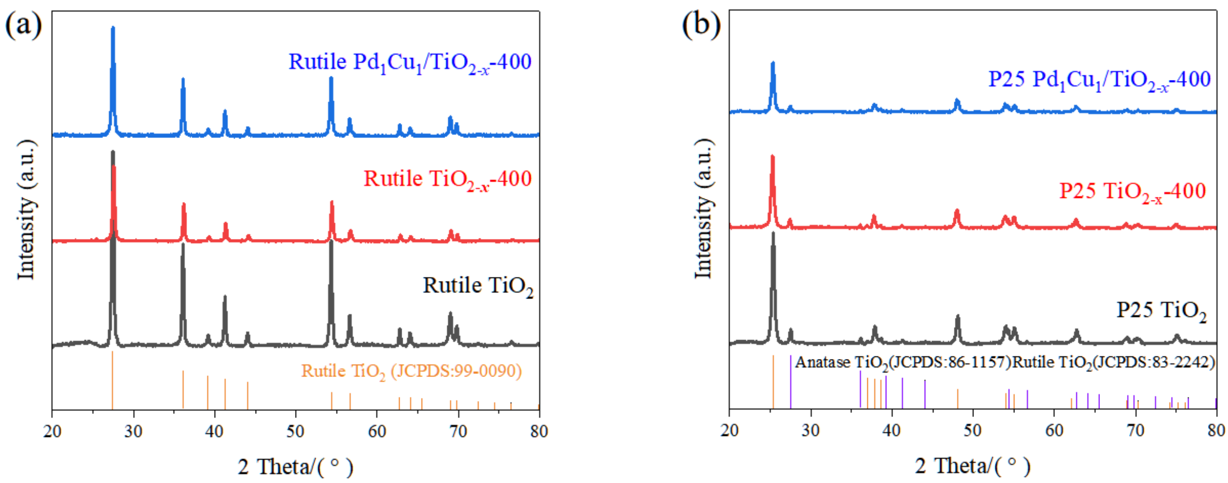

Fig. S7. XRD patterns of a series of different crystal phases (a) XRD patterns of rutile phase series; (b) XRD patterns of P25 series.

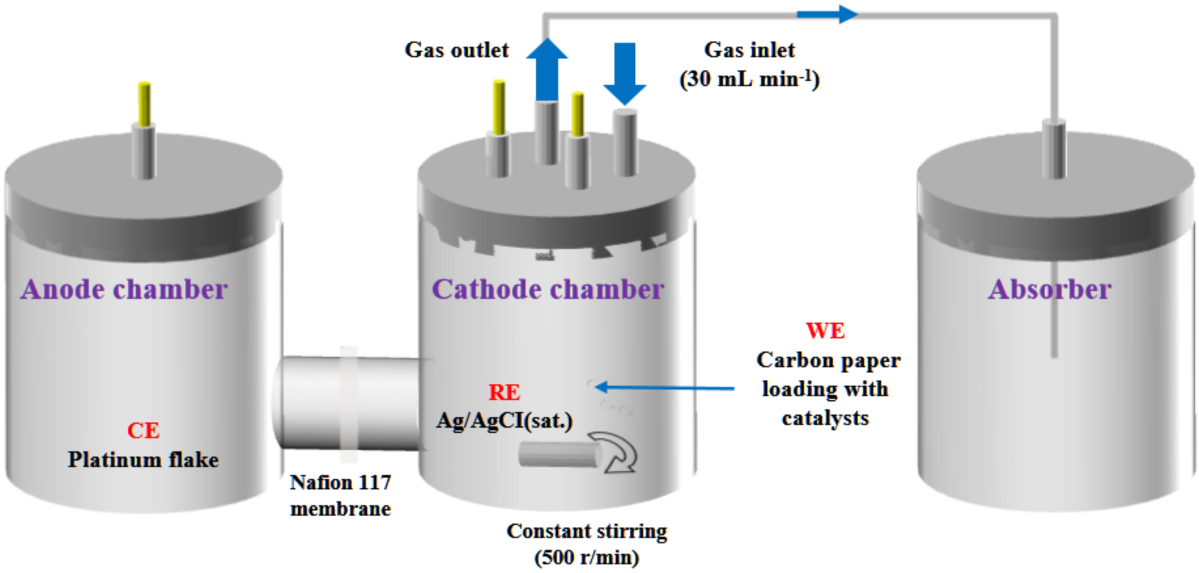

Fig. S8. Schematic diagram of a H-type electrolytic cell with a three-electrode system.

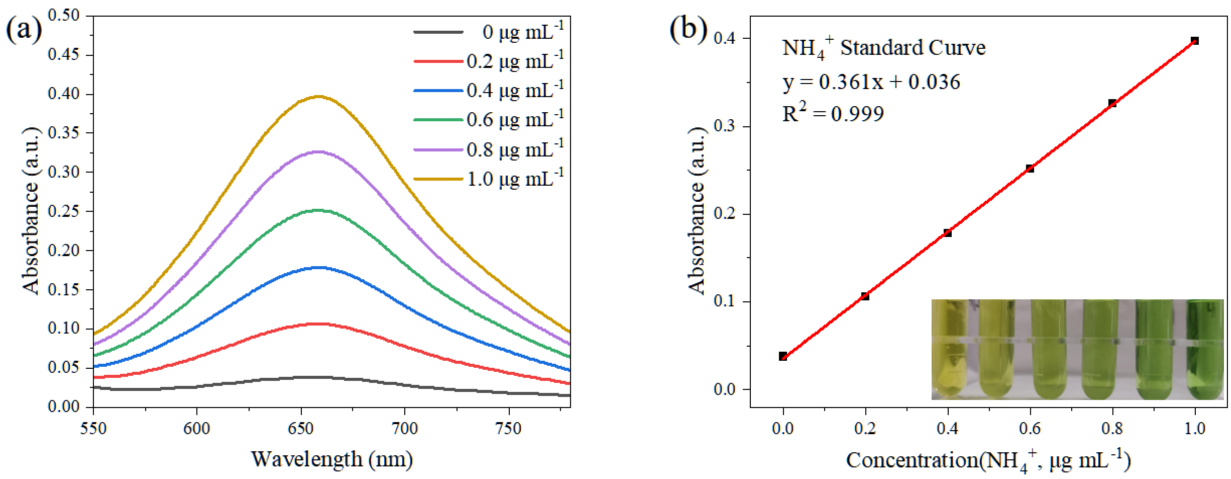

Fig. S9. Quantitative determination of NH_3 concentration based on indophenol blue method. (a) UV-vis absorption spectra of NH_4^+ standard solutions with specified concentrations; (b) NH_4^+ Standard curve in 0.1 mol/L HCl of specified concentrations.

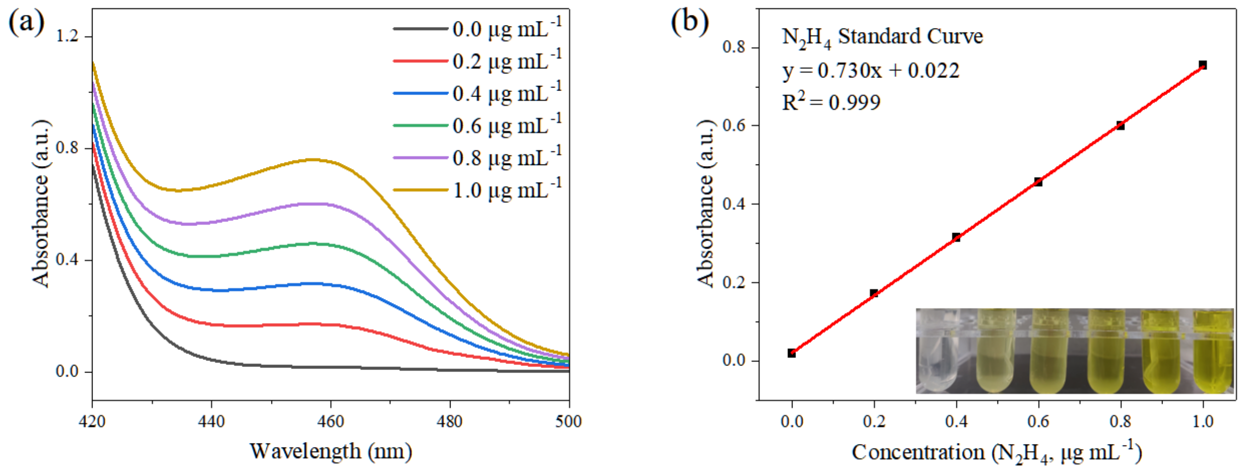

Fig. S10. Quantitative determination of N_2H_4 concentration. (a) UV-vis absorption spectra of N_2H_4 standard solutions with specified concentrations; (b) N_2H_4 Standard curve in 0.1 mol/L HCl of specified concentrations.

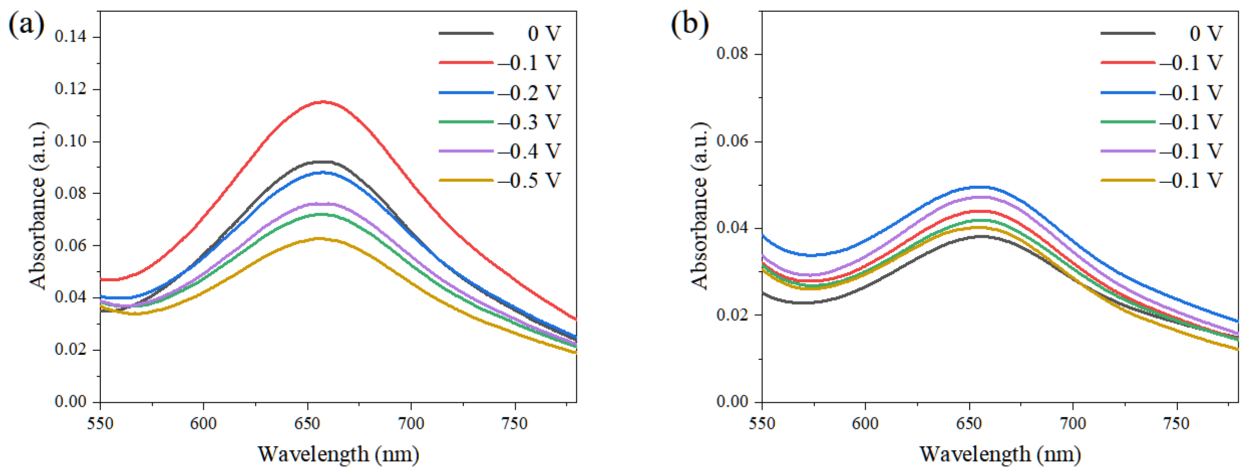

Fig. S11. (a) Uv-vis absorption spectra of electrolytes in cathode chamber after chronoamperometry test of Pd_1Cu_1/TiO_{2-x}-400 catalyst in the potential range of 0~–0.5 V *vs.* RHE. (b) UV-vis absorption spectra of absorption solutions after chronoamperometry test of Pd_1Cu_1/TiO_{2-x}-400 catalyst in the potential range of 0~–0.5 V *vs.* RHE.

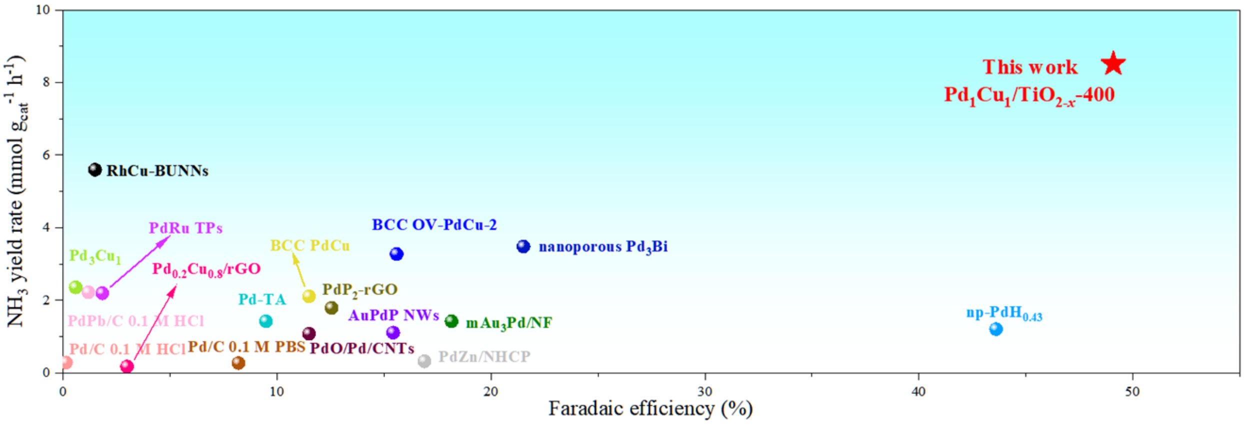

Fig. S12 Comparison of the NRR performance of the Pd_1Cu_1/TiO_{2-x}-400 catalyst with other palladium-based catalysts and their alloy catalysts reported to date under ambient conditions.

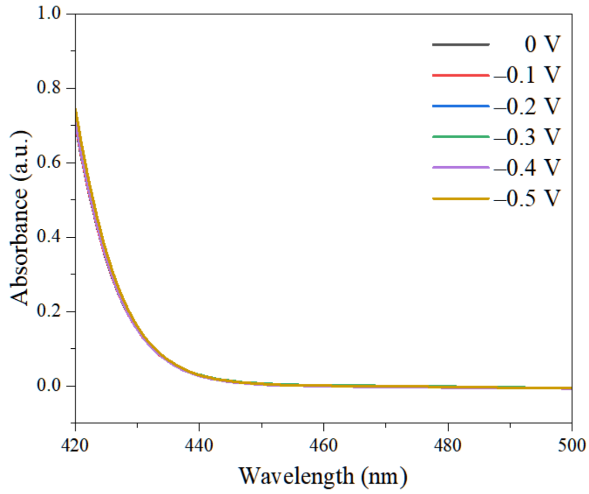

Fig. S13. The N_2H_4 UV-vis absorption spectra of electrolytes at different potentials.

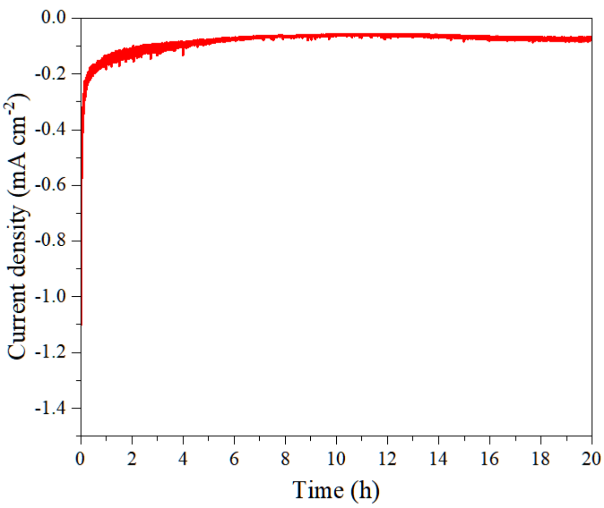

Fig. S14. chronoamperometry stability test of 20 h in 0.1 mol/L HCl under ambient conditions.

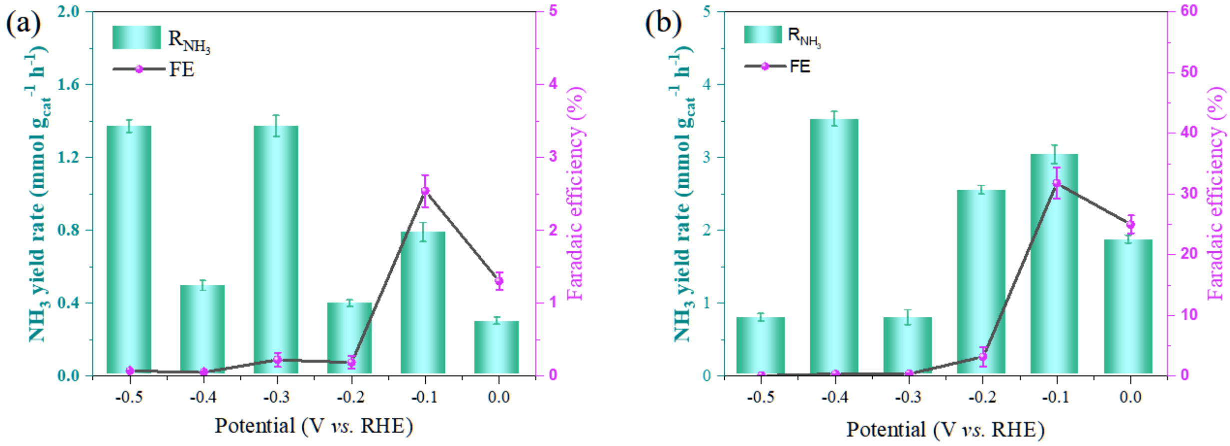

Fig. S15. (a) Electrocatalytic NRR performance of the Pd_1Cu_1/TiO_{2-x}-200; (b) Electrocatalytic NRR performance of the Pd_1Cu_1/TiO_{2-x}-600.

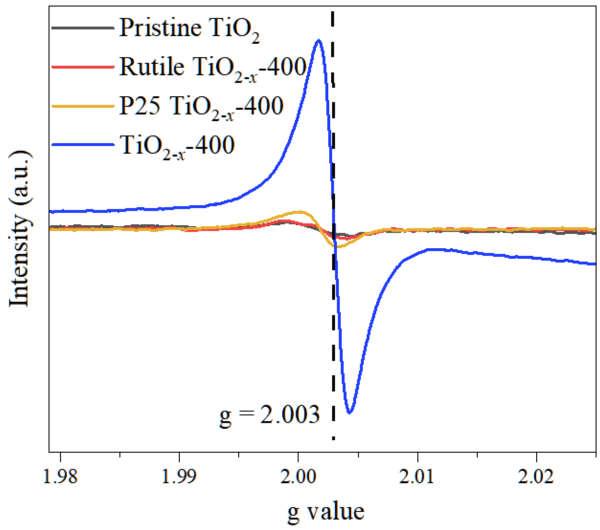

Fig. S16. EPR spectra of pristine TiO_2, Rutile TiO_{2-x}-400, P25 TiO_{2-x}-400, and TiO_{2-x}-400.

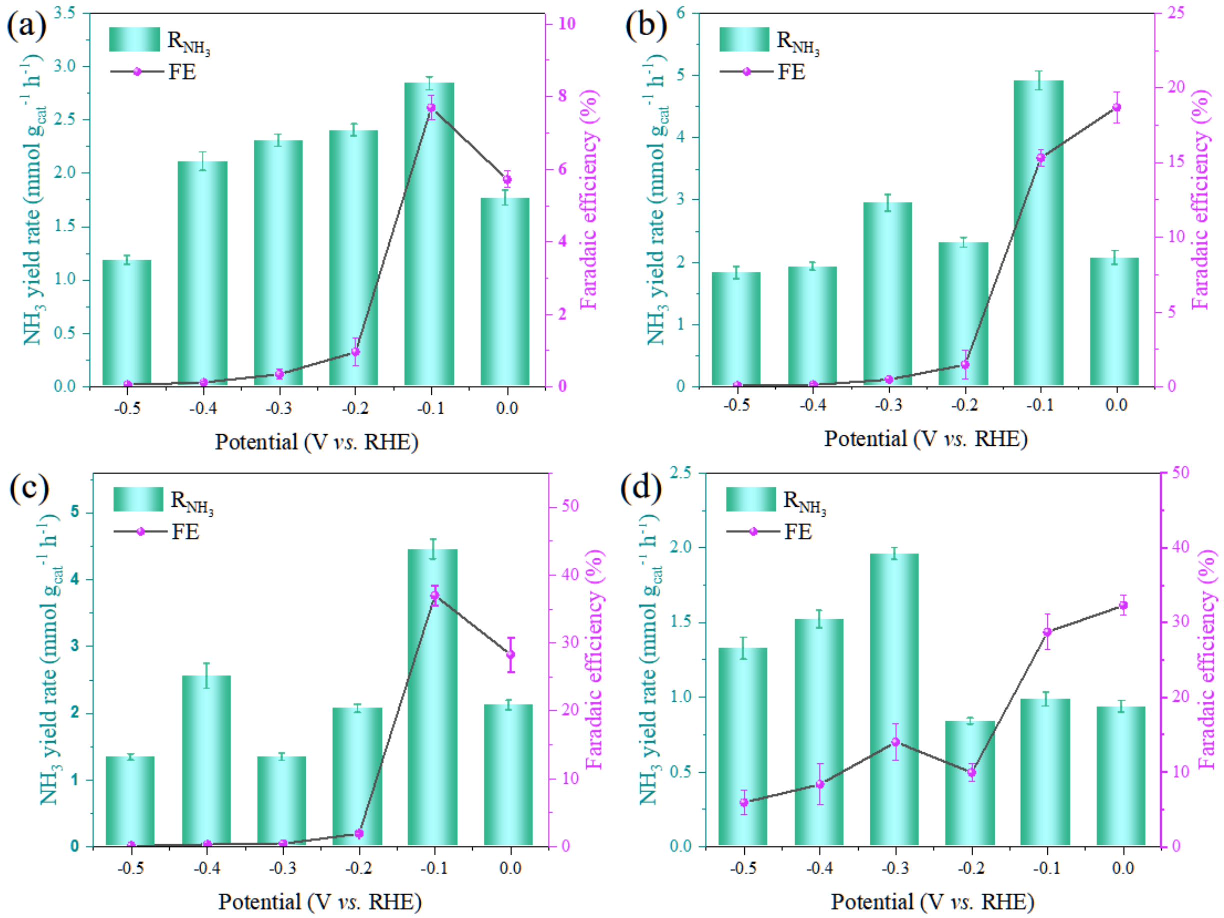

Fig. S17. (a) Electrocatalytic NRR performance of the pristine Pd/TiO_{2-x}-400; (b) Electrocatalytic NRR performance of the Pd_2Cu_1/TiO_{2-x}-400; (c) Electrocatalytic NRR performance of the Pd_1Cu_2/TiO_{2-x}-400; (d) Electrocatalytic NRR performance of the Cu/TiO_{2-x}-400.

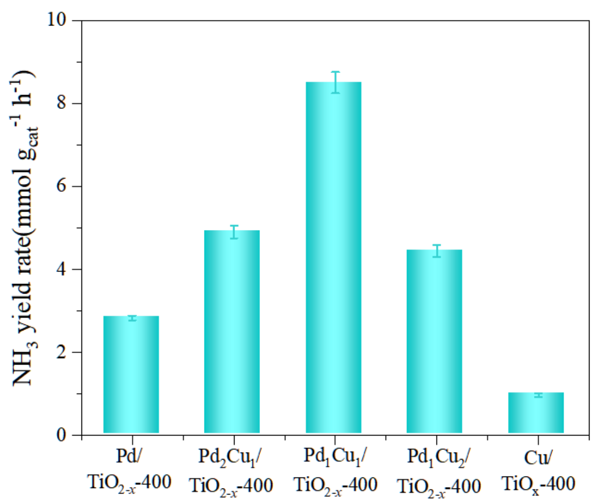

Fig. S18. NH_3 yield rate of the Pd_xCu_y/TiO_{2-x}-400 of various metal mole ratios.

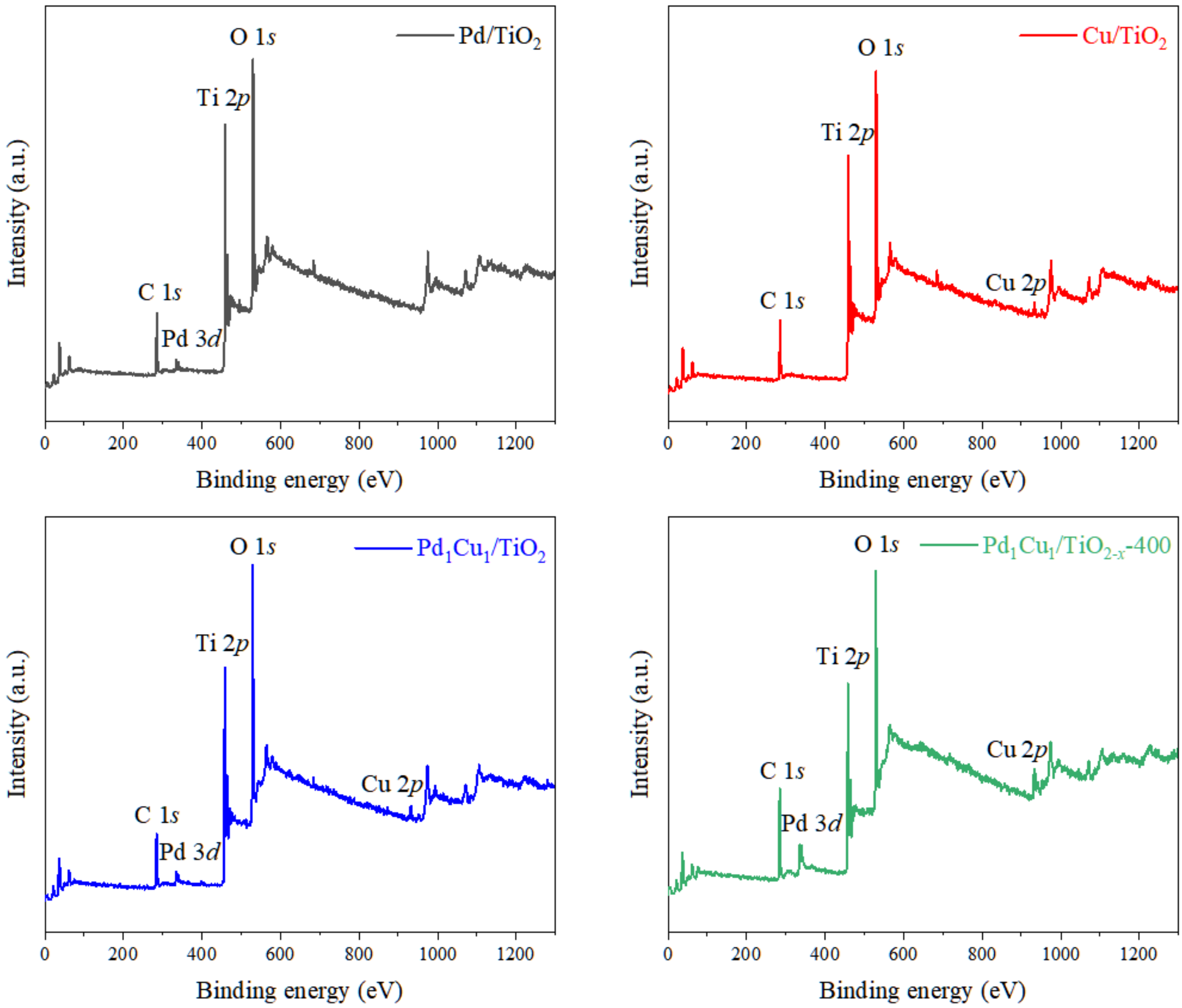

Fig. S19. Full high-resolution XPS spectra of (a) Pd/TiO_2; (b) Cu/TiO_2; (c) Pd_1Cu_1/TiO_2; (d) $Pd_1Cu_1/TiO_{2\text{-}x}$-400.

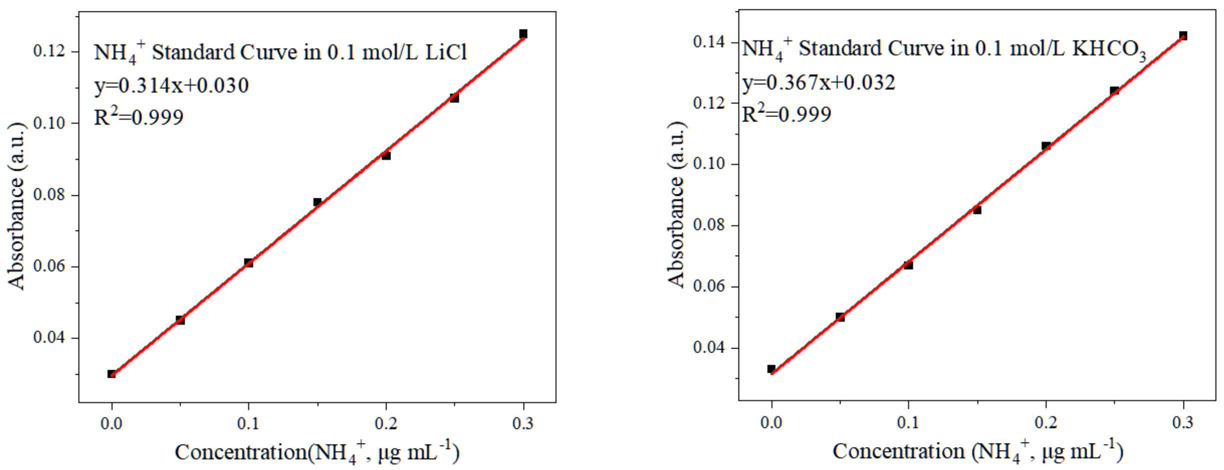

Fig. S20. (a) NH_4^+ Standard curve in 0.1 mol/L LiCl of specified concentrations; (b) NH_4^+ Standard curve in 0.1 mol/L $KHCO_3$ of specified concentrations.

Table S1 Details for synthesis of PdCu/TiO_{2-x}-400 electrocatalysts with various metal molar ratios.

Catalyst	$PdCl_2$ (μL, 5 mg mL^{-1})	$CuCl_2 \cdot 2H_2O$ (μL, 5 mg mL^{-1})	TiO_{2-x}-400 (mg)	$NaBH_4$ solution (10 mg mL^{-1})
Pd/TiO_{2-x}-400	510	0		
Pd_2Cu_1/TiO_{2-x}-400	340	164		
Pd_1Cu_1/TiO_{2-x}-400	256	246	60	10
Pd_1Cu_2/TiO_{2-x}-400	170	328		
Cu/TiO_{2-x}-400	0	492		

Table S2 Details for synthesis of Pd_1Cu_1/TiO_{2-x}-400 electrocatalysts with various metal loadings.

Catalyst	$PdCl_2$ (μL, 5 mg mL^{-1})	$CuCl_2 \cdot 2H_2O$ (μL, 5 mg mL^{-1})	TiO_{2-x}-400 (mg)	$NaBH_4$ solution (10 mg mL^{-1})
1 wt%-Pd_1Cu_1/TiO_{2-x}-400	128	123		
2 wt%-Pd_1Cu_1/TiO_{2-x}-400	256	246		
3 wt%-Pd_1Cu_1/TiO_{2-x}-400	384	369	60	10
4 wt%-Pd_1Cu_1/TiO_{2-x}-400	512	492		
5 wt%-Pd_1Cu_1/TiO_{2-x}-400	640	615		

Table S3 Weight quantifications of PdCu/TiO_{2-x}-400 with various metal molar ratios based on ICP-MS.

Catalyst	Loading (wt%) Pd	Loading (wt%) Cu	Molar ratio	Practical structure
Pd/TiO_{2-x}-400	2.26	0.00	/	Pd/TiO_{2-x}-400
Pd_2Cu_1/TiO_{2-x}-400	1.91	0.58	1.98:1	$Pd_{1.98}Cu_1$/TiO_{2-x}-400
Pd_1Cu_1/TiO_{2-x}-400	1.38	0.75	1.10:1	$Pd_{1.10}Cu_1$/TiO_{2-x}-400
Pd_1Cu_2/TiO_{2-x}-400	0.93	1.16	0.48:1	$Pd_{0.48}Cu_1$/TiO_{2-x}-400
Cu/TiO_{2-x}-400	0.00	2.07	/	Cu/TiO_{2-x}-400

Table S4 Weight quantifications of Pd_1Cu_1/TiO_{2-x}-400 with various metal loadings based on ICP-MS..

Catalyst	Loading (wt%) Pd	Loading (wt%) Cu	Molar ratio	Practical structure
1 wt%-Pd_1Cu_1/TiO_{2-x}-400	0.38	0.66	1.03:1	1.04 wt%-$Pd_{1.03}Cu_1$/TiO_{2-x}-400
2 wt%-Pd_1Cu_1/TiO_{2-x}-400	1.38	0.75	1.10:1	2.13 wt%-$Pd_{1.10}Cu_1$/TiO_{2-x}-400
3 wt%-Pd_1Cu_1/TiO_{2-x}-400	1.31	2.26	1.03:1	3.57 wt%-$Pd_{1.03}Cu_1$/TiO_{2-x}-400
4 wt%-Pd_1Cu_1/TiO_{2-x}-400	1.56	2.66	1.02:1	4.23 wt%-$Pd_{1.02}Cu_1$/TiO_{2-x}-400
5 wt%-Pd_1Cu_1/TiO_{2-x}-400	1.90	3.35	1.05:1	5.25 wt%-$Pd_{1.05}Cu_1$/TiO_{2-x}-400

Table S5 Comparison of the NRR performance of the Pd_1Cu_1/TiO_{2-x}-400 catalyst with other palladium-based catalysts and their alloy catalysts reported to date under ambient conditions

Catalyst	Electrolyte	Potential (V *vs.* RHE)	NH_3 yield rate (mmol g_{cat}^{-1} h^{-1})	Faradaic efficiency (%)	References
Pd_1Cu_1/TiO_{2-x}-400	0.1 M HCl	-0.10	8.51	49.09	This work
Pd-TA	0.1 M Na_2SO_4	-0.45	1.42	9.49	5
Pd/C	0.1 M PBS	-0.05	0.26	8.20	6
Pd/C	0.1 M HCl	-0.05	0.28	0.15	7
PdPb/C	0.1 M HCl	-0.05	2.22	1.19	7
PdO/Pd/CNTs	0.1 M NaOH	0.10	1.07	11.50	8
PdP_2-rGO	0.5 M $LiClO_4$	-0.10	1.78	12.56	9
nanoporous Pd_3Bi	0.05 M H_2SO_4	-0.20	3.47	21.52	10
np-$PdH_{0.43}$	0.1 M PBS	-0.15	1.20	43.6	11
$Pd_{0.2}Cu_{0.8}$/rGO	0.1 M KOH	-0.20	0.16	3.00	12
Nanoporous Pd_3Cu_1	1 M KOH	-0.25	2.35	0.60	13
RhCu-BUNNs	0.1 M KOH	-0.20	5.59	1.50	14
mAu_3Pd/NF	0.1 M Na_2SO_4	-0.10	1.41	18.16	15
BCC PdCu	0.5 M LiCl	-0.10	2.10	11.50	16
AuPdP NWs	0.1 M Na_2SO_4	-0.30	1.10	15.44	17
PdRu TPs	0.1 M KOH	-0.20	2.19	1.85	18
PdZn/NHCP	0.1 M PBS	-0.20	0.31	16.9	19
BCC OV-PdCu-2	0.1 M Li_2SO_4	0.00	3.27	15.6	20

References

1. Z. Geng, Y. Liu, X. Kong, P. Li, K. Li, Z. Liu, J. Du, M. Shu, R. Si and J. Zeng, Achieving a record-high yield rate of 120.9 $\mu g_{NH3}\, mg_{cat}^{-1}\, h^{-1}$ for N_2 electrochemical reduction over Ru single-atom catalysts, *Adv. Mater.*, 2018, **30**, 1803498.
2. L. L. Zhang, L. X. Ding, G. F. Chen, X. F. Yang and H. H. Wang, Ammonia synthesis under ambient conditions: selective electroreduction of dinitrogen to ammonia on black phosphorus nanosheets, *Angew. Chem. Int. Ed.*, 2019, **58**, 2612-2616.
3. Z. W. Fang, P. Wu, Y. M. Qian and G. H. Yu, Gel-derived amorphous bismuth-nickel alloy promotes electrocatalytic nitrogen fixation via optimizing nitrogen adsorption and activation, *Angew. Chem. Int. Ed.*, 2021, **60**, 4275-4281.
4. C. Y. Yang, B. L. Huang, S. X. Bai, Y. G. Feng, Q. Shao and X. Q. Huang, A generalized surface chalcogenation sstrategy for boosting the electrochemical N_2 fixation of metal nanocrystals, *Adv. Mater.*, 2020, **32**, 2001267.
5. G. R. Deng, T. Wang, A. A. Alshehri, K. A. Alzahrani, Y. Wang, H. J. Ye, Y. L. Luo and X. P. Sun, Improving the electrocatalytic N_2 reduction activity of Pd nanoparticles through surface modification, *J. Mater. Chem. A*, 2019, **7**, 21674-21677.
6. J. Wang, L. Yu, L. Hu, G. Chen, H. L. Xin and X. F. Feng, Ambient ammonia synthesis via palladium-catalyzed electrohydrogenation of dinitrogen at low overpotential, *Nat. Commun.*, 2018, **9**, 1795.
7. H. Zhao, D. Zhang, Z. Wang, Y. Han, X. Sun, H. Li, X. Wu, Y. Pan, Y. Qin, S. Lin, Z. Xu, J. Lai and L. Wang, High-performance nitrogen electroreduction at low overpotential by introducing Pb to Pd nanosponges, *Appl. Catal. B*, 2020, **265**, 118481.
8. J. L. Lv, S. L. Wu, Z. F. Tian, Y. X. Ye, J. Liu and C. H. Liang, Construction of PdO-Pd interfaces assisted by laser irradiation for enhanced electrocatalytic N_2 reduction reaction, *J. Mater. Chem. A*, 2019, **7**, 12627-12634.
9. H. T. Xie, Q. Geng, X. J. Zhu, Y. L. Luo, L. Chang, X. B. Niu, X. F. Shi, A. M. Asiri, S. Y. Gao, Z. M. Wang and X. P. Sun, PdP_2 nanoparticles-reduced graphene oxide for electrocatalytic N_2 conversion to NH_3 under ambient conditions, *J. Mater. Chem. A*, 2019, **7**, 24760-24764.
10. X. J. Wang, M. Luo, J. Lan, M. Peng and Y. W. Tan, Nanoporous intermetallic Pd_3Bi for efficient electrochemical nitrogen reduction, *Adv. Mater.*, 2021, **33**, 2007733.
11. W. Xu, G. Fan, J. Chen, J. Li, L. Zhang, S. Zhu, X. Su, F. Cheng and J. Chen, Nanoporous palladium hydride for electrocatalytic N_2 reduction under ambient conditions, *Angew. Chem. Int. Ed.*, 2020, **59**, 3511-3516.
12. M. M. Shi, D. Bao, S. J. Li, B. R. Wulan, J. M. Yan and Q. Jiang, Anchoring PdCu amorphous nanocluster on graphene for electrochemical reduction of N_2 to NH_3 under ambient conditions in aqueous solution, *Adv. Energy Mater.*, 2018, **8**, 1800124.
13. F. Pang, Z. Wang, K. Zhang, J. He, W. Zhang, C. Guo and Y. Ding, Bimodal nanoporous Pd_3Cu_1 alloy with restrained hydrogen evolution for stable and high yield electrochemical nitrogen reduction, *Nano Energy*, 2019, **58**, 834-841.
14. J. Bai, H. Huang, F.-M. Li, Y. Zhao, P. Chen, P.-J. Jin, S.-N. Li, H.-C. Yao, J.-H. Zeng and Y. Chen, Glycerol oxidation assisted electrocatalytic nitrogen reduction: ammonia and glyceraldehyde co-production on bimetallic RhCu ultrathin nanoflake nanoaggregates, *J. Mater. Chem. A*, 2019, **7**, 21149-21156.
15. H. Yu, Z. Wang, S. Yin, C. Li, Y. Xu, X. Li, L. Wang and H. Wang, Mesoporous Au_3Pd film on Ni foam: a self-supported electrocatalyst for efficient synthesis of ammonia, *ACS Appl. Mater. Interfaces*, 2020, **12**, 436-442.
16. W. Tong, B. L. Huang, P. T. Wang, L. G. Li, Q. Shao and X. Q. Huang, Crystal-phase-engineered PdCu electrocatalyst for enhanced ammonia synthesis, *Angew. Chem. Int. Ed.*, 2020, **59**, 2649-

2653.
17. H. Wang, D. Yang, S. Liu, S. Yin, Y. Xu, X. Li, Z. Wang and L. Wang, Metal-nonmetal one-dimensional electrocatalyst: AuPdP nanowires for ambient nitrogen reduction to ammonia, *ACS Sustainable Chem. Eng.*, 2019, **7**, 15772-15777.
18. H. Wang, Y. Li, C. Li, K. Deng, Z. Wang, Y. Xu, X. Li, H. Xue and L. Wang, One-pot synthesis of bi-metallic PdRu tripods as an efficient catalyst for electrocatalytic nitrogen reduction to ammonia, *J. Mater. Chem. A*, 2019, **7**, 801-805.
19. M. Ma, X. Han, H. Li, X. Zhang, Z. Zheng, L. Zhou, J. Zheng, Z. Xie, Q. Kuang and L. Zheng, Tuning electronic structure of PdZn nanocatalyst via acid-etching strategy for highly selective and stable electrolytic nitrogen fixation under ambient conditions, *Appl. Catal. B*, 2020, **265**, 118568.
20. Z. C. Wang, X. K. Wu, J. Liu, D. Zhang, H. Zhao, X. Y. Zhang, Y. N. Qin, N. Z. Nie, D. Wang, J. P. Lai and L. Wang, Ordered vacancies on the body-centered cubic PdCu nanocatalysts, *Nano Lett.*, 2021, **21**, 9580-9586.